Room Temperature Optical Picocavities below 1nm^3 accessing Single Atom Geometries

Cloudy Carnegie[1]*, Jack Griffiths[1]*, Bart de Nijs[1], Charlie Readman[1,2], Rohit Chikkaraddy[1], William M. Deacon[1], István Szabó[3], Edina Rosta[3], Yao Zhang[4], Javier Aizpurua[4], Jeremy J. Baumberg[1+]

[1] NanoPhotonics Centre, Cavendish Laboratory, Department of Physics, JJ Thompson Avenue, University of Cambridge, Cambridge, CB3 0HE, UK
[2] Melville Laboratory for Polymer Synthesis, Department of Chemistry, University of Cambridge, Lensfield Road, Cambridge CB2 1EW, UK
[3] Department of Chemistry, King's College London, 7 Trinity Street, London SE1 1DB, United Kingdom
[4] Materials Physics Center CSIC-UPV/EHU and Donostia International Physics Center DIPC, Paseo Manuel de Lardizabal, 20018 Donostia-San Sebastiàn, Spain

*These authors contributed equally to this work
[+] email: jjb12@cam.ac.uk

Keywords: picocavity, nanocavity, plasmonic cavity, SERS, atomic facet, adatom dynamics

Reproducible confinement of light at the nanoscale is essential for the ability to observe and control chemical reactions at the single-molecule level. Here we reliably form millions of identical nanocavities and show that the light can be further focused down to the sub-nanometre scale via the creation of picocavities - single adatom protrusions with angstrom-level resolution. For the first time we stabilise and analyse these cavities at room temperatures through high-speed surface enhanced Raman on specifically selected molecular components, collecting and analysing more than 2 million spectra. Data obtained on these picocavities allows us to deduce structural information on the nanoscale, showing that thiol binding to gold destabilises the metal surface to optical irradiation. Nitrile moieties are found to stabilise picocavities by ten-fold against their disappearance, surviving typically for more than 1s. Such constructs demonstrate the accessibility of single molecule chemistry under ambient conditions.

Confining optical fields underpins the field of nanophotonics, with implications from nanoscale imaging and transport[1,2], to non-linearities[3], quantum information[4] and nanoscale material engineering[5,6]. The evanescent plasmonic fields supported by negative permittivity metals overcome the diffraction limit and confine light fields to the tens of nanometre scale[7–9]. Particularly useful constructs can trap light into nm-sized gaps between plasmonic components[10,11]. This has enabled optical spectroscopy on picolitre volumes and gives routine access to the single molecule regime[7,12]. More recently, a further level of optical confinement has been revealed due to the localisation of light around a single metal atom within such nano-cavities. Since the rigorously-defined optical volume[13] is now less than a nanometre cubed, these have been termed 'picocavities'. So far these were demonstrated at cryogenic temperatures through the consequent surface-enhanced vibrational spectroscopy of single-molecules[14], as well as in ultrahigh vacuum tip-based spectroscopies[15]. Quantitative measurement of the optical volume can be derived from the nonlinear vibrational coupling observed, allowing the dynamics of molecules to be observed at low temperatures T=10K.

However it was discovered so far that such picocavities were unstable at room temperature[14], making them hard to exploit for such demanding light-matter applications.

Here we demonstrate by surface-enhanced Raman spectroscopy (SERS) that picocavities are visible at room temperature. Although less stable than at cryogenic temperatures, high-speed SERS clearly identifies their formation and decay. We find transient effective molecular temperatures far exceeding 300K, evidencing the optomechanical molecular driving of individual molecules. Although their formation is driven by light, the barrier to their formation and their subsequent stability are affected by the molecules inside the plasmonic gaps used. The routine production of optical fields confined at the atomic scale opens up many new areas of interface science, since catalysis and electrochemistry can now be studied under ambient and realistic conditions.

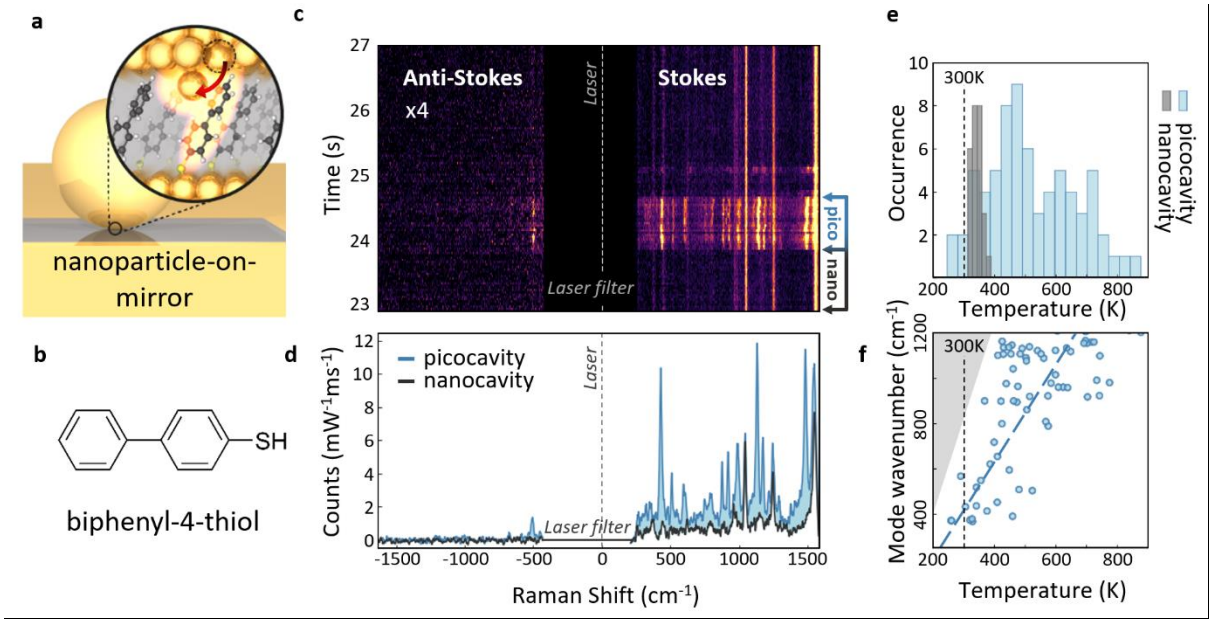

Figure 1. (a) Schematic of nanoparticle-on-mirror (NPoM) geometry. Inset shows formation of picocavity by movement of surface atom to adatom. **(b)** Structure of biphenyl-4-thiol. **(c)** Kinetic SERS spectrum from NPoM showing stable bulk BPT in nanocavity (grey bracket on right) as well as few-molecule picocavity event (blue bracket). **(d)** SERS spectra from a nanocavity and a picocavity instantaneous configuration. **(e)** Extracted effective temperatures for both picocavities and nanocavities, collected from >1000 NPoM constructs. **(f)** Correlation between effective temperature of picocavity and wavenumber of vibrational mode in which it is estimated. Blue dashed line is guide to the eye. Grey region shows signal-to-noise limit.

To develop formation of these picocavities, we first create reliable nanocavities formed in the gap between two plasmonic components. Millions of nanoparticle-on-mirror (NPoM) constructs are produced on each sample by nano self-assembly. Each consists of a single gold nanoparticle spaced above a flat gold film by a molecular spacer layer and acts analogously to a plasmonic dimer due to the coupling of electrons in the nanoparticle to image charges in the film below[16]. Optical fields are tightly confined inside the gap d, with mode volumes of $V_I \simeq Rd^2/n_g^2$ = 40-100 nm^3 set by the radius of nanoparticle R, and spacer refractive index n_g.

At low temperatures, we showed the formation of picocavities[14] with greatly reduced mode volume compared to these nanocavities. They are created when laser irradiation of a NPoM induces single gold adatoms to extrude from the crystalline bulk gold facets around the gap, resulting in an effective cavity volume of 1nm^3 or less (Figure 1a). Self-assembled monolayers (SAMs) are used as spacer layers since they very robust and close-packed[17–20], excluding ions or impurities from the optically-sensitive

gap region and allowing stable spectroscopy. In the work here two thiol-linked stable SAMs are used. Biphenyl-4-thiol (BPT) attaches to the flat gold bottom surface with its methyl head group in close proximity to the gold nanoparticle above. Chemically similar is 4'-cyanobiphenyl-4-thiol (NC-BPT) which instead has a cyanide triple bond as the head group positioned near the nanoparticle, giving an unambiguous Raman vibrational marker between 2000-2500 cm^{-1} which can be used to locate the Au atom. These molecules both have large Raman cross sections, making them ideal Raman probes and avoiding complications from fluorescent tagging.

When a picocavity is formed, the single gold adatom leads to a further local enhancement of the optical field strength via an atomic-scale 'lightning rod' effect[21]. The resulting field enhancement $E{\sim}4$ produces a SERS enhancement $E^4 > 200$, which exceeds that of all other (∼100) molecules within our gap 'hotspot', resulting in single molecule SERS on both the Stokes and anti-Stokes sides of the spectra. In addition, the picocavities produce a strong field gradient across each bond within the single molecule underneath, breaking the selection rules that keep its IR-active modes dark in Raman, and turning on a new set of SERS lines which depend on the precise relative positions of atom and molecule on the Å scale[14,22].

Since at room temperature these picocavities are often fleeting and hard to stabilise, we develop here an experimental protocol to investigate the dynamics and characteristics of these events in ambient conditions, using SERS to investigate vibrational dynamics at the nanoscale. NPoM constructs are irradiated with a 633nm HeNe laser while continuously collecting the Raman scattered light on a cooled CCD in continuous readout mode (see methods). We reduce integration times to 10 ms, well below the >1s typically used. This allows the fast picocavity dynamics to be directly observed in time (Figure 1c). On the Stokes (right) side, the typical fingerprint of persistent BPT Raman lines from the 100 molecules in the nanocavity can be seen, with lines unchanging in time. The minimal spectral wandering in these lines evidences the robust characteristics of the SAM (a representative spectrum is grey in Figure 1d). Picocavity events are recognised by the multitude of extra lines that transiently appear across the spectra for short bursts (see between t=24-25s in Figure 1c). The <4cm^{-1} spectral wandering observed comes from slight <Å movements of the gold adatom as well as from slight flexing or charge movements in the very few (or single) molecule(s) in the high field gradient around the adatom (blue spectrum Figure 1d).

Single-atom SERS elicited from picocavities is likely at the root of many transient observations over several decades of SERS and TERS measurements on a wide variety of nanostructured surfaces[15,23–25]. Here it is identified in single nanostructures in precisely controlled conditions, allowing its careful investigation thus opening up systematic approaches to its exploitation.

The Stokes scattered Raman light of BPT molecules excited mostly from a vibrational ground state to a higher vibrational state dominates the spectra. However anti-Stokes scattered photons can also be seen, which requires a molecule to already be in a vibrationally-excited state when excited by the laser[14,26]. The probability of occupying excited states decreases with the energy of the vibrational mode, so at room temperature anti-Stokes peaks are weak and only visible for low wavenumber modes close to the laser wavelength. Even these are invisible for the persistent nanocavity spectra of 100 molecules in the NPoM (Figure 1d, grey). However, when a picocavity is formed the phonon population in the selected single molecule out is optomechanically pumped to the higher state[14], so that some anti-Stokes lines are now visible (Figure 1d).

The anti-Stokes to Stokes (AS/S) intensity ratio yields an effective temperature for each optomechanically-pumped vibrational mode, characterizing the temperature that would achieve this excited state population thermally in the absence of any pumping. The local temperature of the

surrounding SAM molecules in the nanocavity, calculated from the AS/S ratio of the persistent lines, is only possible when using much longer time-averages (>30s, see SI). This average local nanogap temperature of 341K (Figure 1e) has a narrow distribution (grey) consistent across all NPoMs analysed. In comparison the effective temperatures extracted from picocavity lines show a much broader hot distribution, revealing the differences in vibrational coupling strength from the range of adatom-molecule distances. Interestingly, higher temperatures are found for the high-wavenumber modes (Figure 1f). Together with the observed variability in vibrational energies of the picocavity lines, this shows how sub-nanometre resolution measurements are now enabled at room temperature.

The single-molecule effective vibrational temperatures extracted at room temperature (400-800K) are much lower than for measurements at cryogenic temperatures[14] (>1000K). This is due to the increased thermal depopulation of phonons by nonlinear phonon-phonon scattering when greater thermal vibrational backgrounds are present. As a result, the anti-Stokes emission is weaker and henceforth the Stokes spectra are utilised for exploring the fast dynamics.

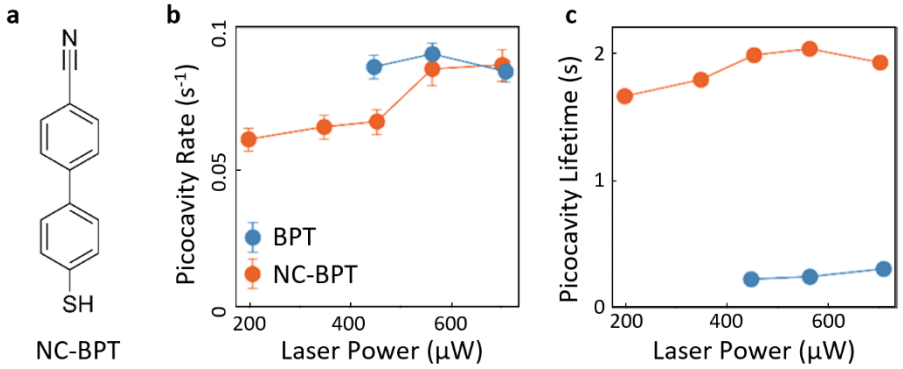

Figure 2. (a) Structure of 4'-cyanobiphenyl-4-thiol (NC-BPT). **(b)** Mean rate of picocavity events in ~2500 BPT and NC-BPT SAM NPoM nanocavities with increasing incident 633nm laser power. **(c)** Corresponding mean lifetime of picocavities generated.

The optically-induced formation of picocavities can be stabilised at room temperature by chemically modifying the SAM. Here, over two million SERS spectra are taken of BPT and NC-BPT monolayers incorporated into different NPoM samples, with 1000 consecutive SERS spectra for ~2500 NPoMs across a range of irradiation powers (Figure 2). When detecting picocavity events, transient SERS lines detected for only a single spectrum are discarded to avoid introducing statistical noise. The NC-BPT molecular layer shows a clear power dependence for picocavity formation over the range of incident power investigated (Figure 2b). Similar formation rates of picocavities are found for both molecular spacers at larger incident powers. At lower powers, signal-to-noise constrains the detection of fleeting BPT picocavities. Once picocavities do form, the different chemistry of NC-BPT makes these systems an order of magnitude more stable than BPT against their adatom being reabsorbed back into the Au bulk (Figure 2c). Changes in molecular packing density[27,28] or adatom-molecule configuration may thus be responsible, however the underlying mechanism for the improved stability is yet unclear. This enhanced picocavity stability allows an order of magnitude increase in integration times for each SERS spectrum using NC-BPT which improves the resulting signal-to-noise while still allowing observation of transient events. This allows observation of picocavity generation at lower irradiation powers and enables real-time observations of individual chemical bonds in ambient conditions.

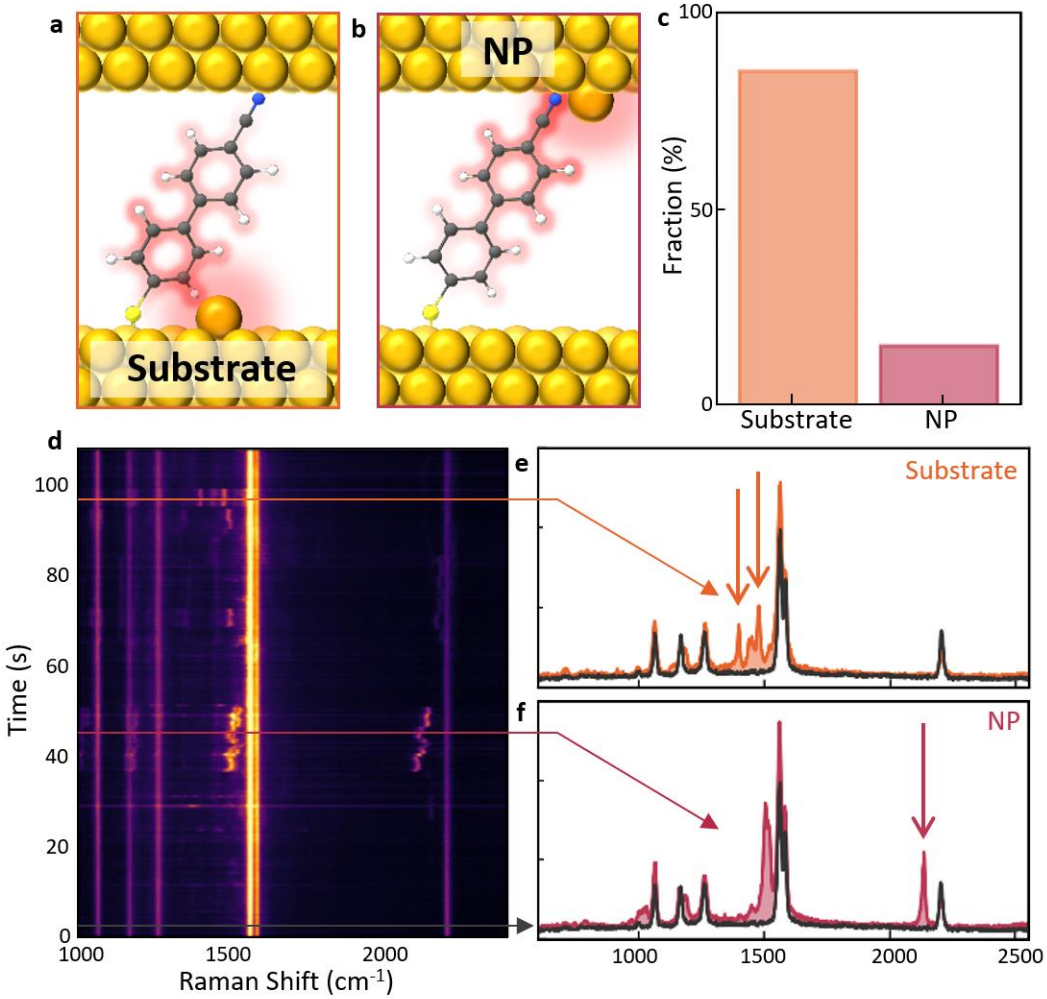

Figure 3. (a,b) Schematic of picocavity adatoms on the Au substrate and nanoparticle facet, giving different interactions with NC-BPT. **(c)** Relative fractions of the two picocavity types observed for 300μw laser power. **(d)** Consecutive SERS spectra showing transient peaks resulting from both forms of picocavity. **(e)** SERS spectra for picocavity adatom on the Au substrate, and **(f)** picocavity adatom on the nanoparticle facet.

Due to the S-Au chemical interaction during SAM formation, each NPoM nanocavity assembles with all molecules orientated with the thiol group bound to the lower gold substrate. For NC-BPT, this leaves the cyanide head groups closest to the nanoparticle and breaks symmetry in our nanogaps (Figure 2a,b). This makes it possible to distinguish between picocavity events where the gold adatom extrudes from the lower planar substrate or from the nanoparticle surface. These two cases generate different field distributions and gradients across the nearest molecule and the molecular asymmetry then leads to the formation of distinct sets of transient spectral peaks (Figure 3e,f; see also density functional theory simulations in SI4). Time-scans of SERS spectra can display both types of picocavity event (Figure 3c), here lasting >10s each. Adatoms extruding from the Au substrate interact mainly with the phenyl rings of the molecule, leading to transient lines in the region ν<1500cm^{-1} (Figure 3d, arrows). In contrast, adatoms extruding from the nanoparticle give significant additional interactions with the high wavenumber C≡N triple bond, resulting in a transient peak ν>2000cm^{-1} (Figure 3e, arrow).

This distinction allows direct comparison of picocavity formation rates for adatoms originating in the substrate or nanoparticle. Analysing data from 262 NPoMs irradiated with 300 μW of 633nm laser light for >100s shows that only 15.1% of detected picocavity events were generated by Au atoms from

the nanoparticle surface (Figure 3f). This implies that such optical-induced forces arise not merely from the deposition of energy into the gold surfaces around the gap, but shows the important role of the SAM and the chemical interactions between functional groups and gold. Current models are not yet able to reproduce these effects, since inter-molecular forces in the SAM as well as interatomic forces in the metals must play key roles. This work opens up a vast landscape to explore the chemistry of metal-atom – molecular binding, which underpins catalysis as well as electrochemistry, and is now accessible in a very wide range of reaction conditions from cryogenic UHV to ambient lab conditions to practical reactors.

In conclusion we have shown that the chemistry and dynamics of single gold adatom movement can be observed and characterised in ambient conditions. We achieve this using robust simple nano-assembled constructs which create nanoscale gaps to tightly confine incident light enabling high temporal resolution SERS measurements that can distinguish chemistry in real time. We note that recent results from TERS likely result from exactly the same picocavity process, but are much more difficult to systematically explore due to the complication of stabilising the tip-sample distance and simultaneously creating the pico-cavities by Au adatom movement. Recent modelling has attempted to specify site position of adatom relative to analytes, but relies on symmetric SAMs and so cannot make the crucial distinction between nanoparticle and surface[29]. By incorporating different molecular monolayers we simultaneously break this symmetry as well as inducing changes in the barrier for gold adatom dynamics, suggesting that chemical stabilisation is an effective approach to more durable cavity formation. We show some of the first investigations into the spectral information emitted during picocavity events and shown that for the NC-BPT system adatoms are more likely to protrude from the underlying flat gold mirror than the gold nanoparticle above.

Methods

Sample Preparation. Atomically smooth Au surfaces are prepared by evaporating 100nm of Au onto Si wafers purchased from Si-Mat. Small silicon pieces are then glued to the wafer using Epo-Tek 377 epoxy glue and the wafer is slowly cooled from 150°C curing temperature to room temperature. Silicon pieces can then be peeled off on demand to reveal a perfectly smooth Au surface. Self-assembled monolayers of BPT and NC-BPT are formed by immersion in 1mM dry ethanol solution for 22hrs. Commercial BBI 80nm Au nanoparticles are then dropcast on the sample to form the NPoM constructs. Samples are rinsed with dionised water and then dried.

SERS Measurements. For BPT SERS measurements, light from a 632.8nm HeNe laser is focused to a diffraction limited spot on the sample using an Olympus LMPlanPLN 100x NA0.8 objective lens. Scattered light is imaged on an Andor Newton EMCCD through an Andor Shamrock 303i-B spectrometer using a 600l/mm diffraction grating with 650nm blaze. For NC-BPT SERS measurements, light from a 633nm diode laser is focused to a diffraction limited spot on the sample using a Zeiss EX Epiplan-Neoluar 100x 0.9NA objective lens. Scattered light is imaged on an Andor Newton EMCCD through a HORIBA Triax 320 spectrometer using a 600l/mm diffraction grating with 750nm blaze. In both cases, elastically scattered light is removed using 2 Thorlabs NF-633-25 notch filters and laser power on sample is measured using Thorlabs PM16-121 power meters.

Acknowledgment
We acknowledge financial support from EPSRC Grants EP/L027151/1 and EP/N020669/1. C.C. acknowledges support from NPL PO443073. B.d.N. acknowledges support from the Leverhulme

Trust and Isaac Newton Trust. R.C. acknowledges financial support from the Junior Research Fellowship from Trinity College.

1. Barnes, W. L., Dereux, A. & Ebbesen, T. W. Surface plasmon subwavelength optics. *Nature* **424,** 824–830 (2003).

2. Delamarche, E. & Michel, B. Structure and stability of self-assembled monolayers. *Thin Solid Films* **273,** 54–60 (1996).

3. Kauranen, M. & Zayats, A. V. Nonlinear plasmonics. *Nat. Photonics* **6,** 737 (2012).

4. Tame, M. S. *et al.* Quantum plasmonics. *Nat. Phys.* **9,** 329–340 (2013).

5. Brongersma, M. L., Halas, N. J. & Nordlander, P. Plasmon-induced hot carrier science and technology. *Nat. Nanotechnol.* **10,** 25–34 (2015).

6. Ebbesen, T. W. Hybrid Light–Matter States in a Molecular and Material Science Perspective. *Acc. Chem. Res.* **49,** 2403–2412 (2016).

7. Chikkaraddy, R. *et al.* Single-molecule strong coupling at room temperature in plasmonic nanocavities. *Nature* **535,** 127–130 (2016).

8. Koenderink, A. F., Alù, A. & Polman, A. Nanophotonics: shrinking light-based technology. *Science* **348,** 516–21 (2015).

9. Savage, K. J. *et al.* Revealing the quantum regime in tunnelling plasmonics. *Nature* **491,** 574–577 (2012).

10. Chikkaraddy, R. *et al.* How Ultranarrow Gap Symmetries Control Plasmonic Nanocavity Modes: From Cubes to Spheres in the Nanoparticle-on-Mirror. *ACS Photonics* **4,** 469–475 (2017).

11. Zhu, W. *et al.* Quantum mechanical effects in plasmonic structures with subnanometre gaps. *Nat. Commun.* **7,** 11495 (2016).

12. Chikkaraddy, R. *et al.* Mapping Nanoscale Hotspots with Single-Molecule Emitters Assembled into Plasmonic Nanocavities Using DNA Origami. *Nano Lett.* **18,** 405–411 (2018).

13. Sauvan, C., Hugonin, J. P., Maksymov, I. S. & Lalanne, P. Theory of the Spontaneous Optical Emission of Nanosize Photonic and Plasmon Resonators. *Phys. Rev. Lett.* **110,** 237401 (2013).

14. Benz, F. *et al.* Single-molecule optomechanics in 'picocavities'. *Science (80-.).* **354,** 726–729 (2016).

15. Zhang, R. *et al.* Chemical mapping of a single molecule by plasmon-enhanced Raman scattering. *Nature* **498,** 82–86 (2013).

16. Tserkezis, C. *et al.* Hybridization of plasmonic antenna and cavity modes: Extreme optics of nanoparticle-on-mirror nanogaps. *Phys. Rev. A* **92,** 053811 (2015).

17. Love, J. C., Estroff, L. A., Kriebel, J. K., Nuzzo, R. G. & Whitesides, G. M. Self-assembled monolayers of thiolates on metals as a form of nanotechnology. *Chemical Reviews* **105,** 1103–1169 (2005).

18. Pensa, E. *et al.* The Chemistry of the Sulfur–Gold Interface: In Search of a Unified Model. *Acc. Chem. Res.* **45,** 1183–1192 (2012).

19. Häkkinen, H. The gold–sulfur interface at the nanoscale. *Nat. Chem.* **4,** 443–455 (2012).

20. Ulman, A. Formation and Structure of Self-Assembled Monolayers. *Chem. Rev.* **45,** 1533–1554 (1996).

21. Urbieta, M. *et al.* Atomic-Scale Lightning Rod Effect in Plasmonic Picocavities: A Classical View to a Quantum Effect. *ACS Nano* **12,** 585–595 (2018).

22. Moskovits, M., Dilella, D. P. & Maynard, K. J. *Surface Raman Spectroscopy of a Number of Cyclic Aromatic Molecules Adsorbed on Silver: Selection Rules and Molecular Reorientation*. *Langmuir* **4,** (1988).

23. Kneipp, K. *et al.* Single molecule detection using surface-enhanced raman scattering (SERS). *Phys. Rev. Lett.* **78,** 1667 (1997).

24. Zhong, J.-H. *et al.* Probing the electronic and catalytic properties of a bimetallic surface with 3 nm resolution. *Nat. Nanotechnol.* **12,** 132–136 (2016).

25. Nie, S. & Emory, S. R. *Probing Single Molecules and Single Nanoparticles by Surface-Enhanced Raman Scattering Downloaded from*. *Science* **275,** (Springer, 1997).

26. Schmidt, M. K., Esteban, R., González-Tudela, A., Giedke, G. & Aizpurua, J. Quantum Mechanical Description of Raman Scattering from Molecules in Plasmonic Cavities. *ACS Nano* **10,** 6291–6298 (2016).

27. Meyerbröker, N. & Zharnikov, M. Modification of Nitrile-Terminated Biphenylthiol Self-Assembled Monolayers by Electron Irradiation and Related Applications. *Langmuir* **28,** 9583–9592 (2012).

28. Matei, D. G., Muzik, H., Gölzhäuser, A. & Turchanin, A. Structural Investigation of 1,1′-Biphenyl-4-thiol Self-Assembled Monolayers on Au(111) by Scanning Tunneling Microscopy and Low-Energy Electron Diffraction. *Langmuir* **28,** 13905–13911 (2012).

29. Shin, H. H. *et al.* Frequency-Domain Proof of the Existence of Atomic-Scale SERS Hot-Spots. *Nano Lett.* **18,** 262–271 (2018).